Characterization of a microwave photonic synthesizer for future applications in radio astronomy instrumentation

Jay Frothingham[1], Bill Shillue[2]

[1] Smith College, Northampton MA
[2] Central Development Laboratory, National Radio Astronomy Observatory, Charlottesville VA

***Abstract* – The performance and characteristics of a new tunable microwave photonic synthesizer were measured and compared against existing radio astronomy instrumentation and specifications. Initial testing verified the synthesizer's delivery of desired functions. Further testing evaluated the stability and noise of the synthesizer's output signal.**

Contents

Background

Within a typical superheterodyne radio telescope receiver, an observed signal will be mixed with a stable reference signal of a set frequency produced by a local oscillator (LO). This mixing process converts the received radio frequency (RF) signal to a lower, intermediate frequency (IF) signal that can be more easily processed, transmitted, and eventually digitized. In an interferometric array, the LO signal also serves to synchronize each individual antenna. The LO frequency can be varied to change the range of frequencies the telescope is able to receive. With a known LO frequency, information about the original signal is preserved. The stability of a local oscillator is important for this reason, and also because different types of noise in an LO signal can impact the RF mixing process and the resulting IF signal.

Figure 1. Local oscillator in antenna.

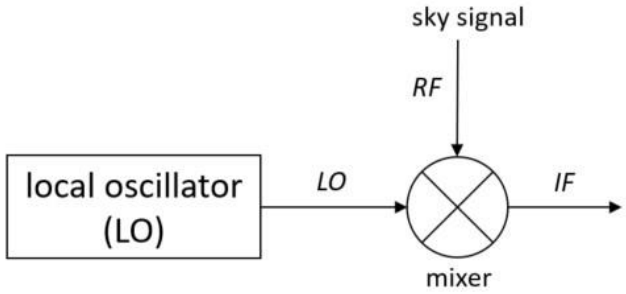

Block diagram of the local oscillator mixing process. A local oscillator (LO) signal mixes with a radio frequency (RF) signal from the sky or target object to produce an intermediate frequency (IF) signal.

Wideband noise can include types of noise such as thermal or shot noise, noise that is distributed over a broad range of frequencies and impacts the signal-to-noise-ratio. Wideband noise present in an LO signal will also appear in the IF signal after mixing with the RF signal. This can worsen the overall noise temperature of the receiver. Sideband noise is found closer to the signal's carrier frequency and impacts the frequency and phase stability of a signal. Sideband noise present in an LO signal can prevent the preservation of phase when coherently combining received sky signals in an antenna array application.

Figure 2. Illustration of phase noise in the time and frequency domains.

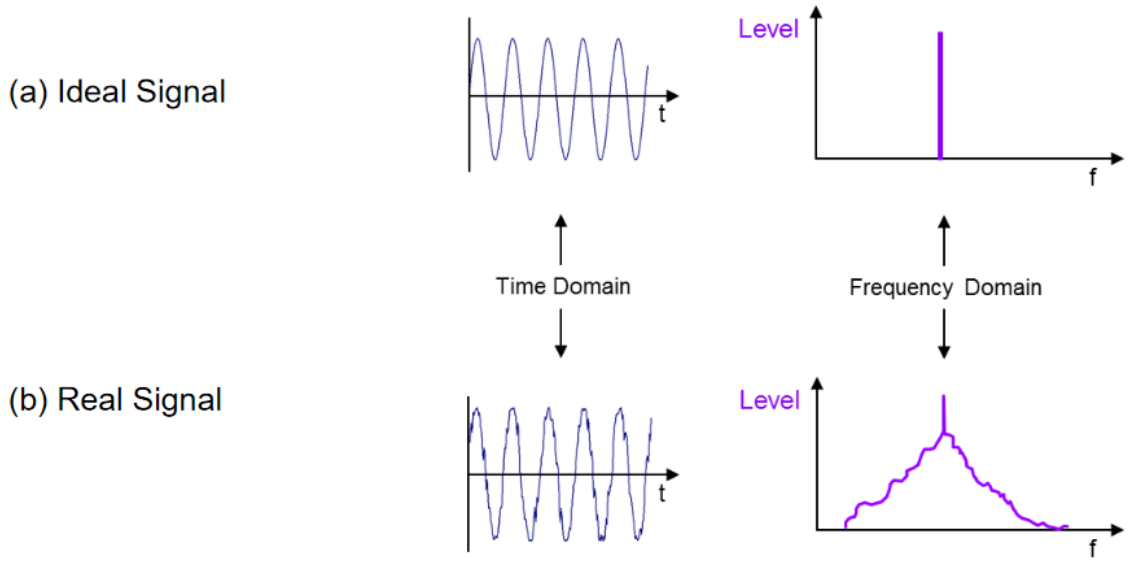

Figure source: Figure 2-1, Rohde & Schwarz. The upper two plots in the figure (a) show the time and frequency domain representations of an ideal single-frequency signal. There is no jitter visible in the time domain, and no spread visible in the frequency domain. The lower two plots in the figure (b) show the time and frequency domain representations of a real signal. The spread-out spectrum visible in the frequency domain is equivalent to the jitter visible in the time domain.

Stability and noise can be quantified by producing phase noise plots, calculating timing jitter, measuring frequency drift, and producing plots of Allan variance. Single-sideband (SSB) phase noise is plotted as a function of frequency offset from the desired or "carrier" frequency. It is calculated by comparing power per Hertz of bandwidth at a particular frequency offset from the carrier frequency to the power at the carrier frequency. A phase noise plot typically shows a decrease in phase noise as the frequency offset increases—i.e., at frequencies further and further away from the carrier signal, there is less power output. Changes in the phase of the signal shift it, resulting in higher power output at offset frequencies than a signal of the same frequency with no changes in phase. Phase noise and timing jitter are analogs of each other in the frequency and time domains, respectively. Each measures the stability of a signal.

Frequency drift is the amount by which the frequency of the signal changes over time. It can be measured as a rate change in frequency. Ideally, frequency drift should be low, meaning significant change in frequency only occurs over very long timescales. Allan variance provides

an estimate of how different types of noise impact the frequency in terms of both long-term and short-term stability. It is calculated by taking readings of frequency deviation, squaring the difference between successive samples, and calculating one half of the time average of those squared differences. Rather than calculating a single value, Allan variance is typically presented as a plot of variance values calculated for different values of sample period τ. Sample period, or averaging time, controls the number of differences taken.

A way to mitigate both stability and noise concerns is with the implementation of a phase-locked loop (PLL). In a PLL, a generated signal is compared to an assumed-to-be-stable reference signal. The difference in phase between the generated signal and the reference signal is kept constant (i.e., the frequencies are locked) by applying a filtered bias voltage proportional to the detected difference in phase, which increases or decreases the frequency of the generated signal as necessary to keep it locked with the reference signal. Typically, the generated signal is produced by a voltage-controlled oscillator (VCO).

Figure 3. Phase-locked loop

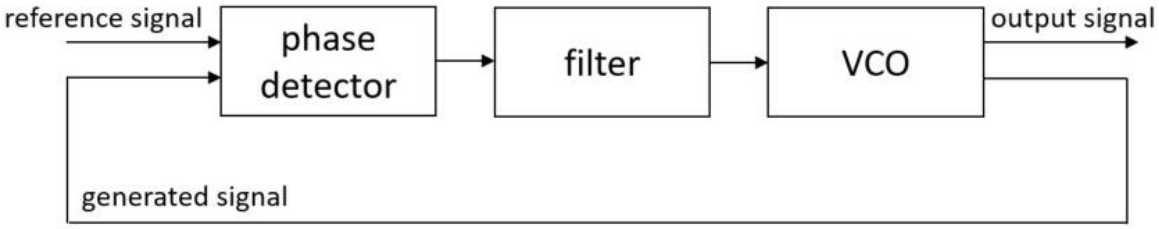

The microwave photonic synthesizer studied in this research project is a two-laser heterodyne source manufactured by OEwaves. It consists of a voltage-controlled oscillator and a laser lock box. In free-running mode, only the VCO is in use. It generates a microwave signal based on input applied through a graphical user interface (GUI), and the frequency of the signal can be finely adjusted to match the desired frequency more closely. However, it is because of the laser lock box that this system is of interest. The laser lock box acts as a phase-locked loop, and is designed to quickly lock the system's output signal at one stable frequency.

The OEwaves system could benefit the ngVLA (Next Generation Very Large Array) project by providing a high-quality laser source. Its small size and weight would reduce contributions to the total size, weight, and power (SWaP) budget. The system is also capable of providing a reference signal over optical fiber, allowing for the possibility of a remote local oscillator. Its high-quality performance on paper and potential benefits warrant further testing to evaluate whether the OEwaves system is suitable for use with ngVLA or other future radio telescopes.

Methods

This project was carried out in three phases: verification of functionality, characterization of stability, and comparison to ALMA and ngVLA specifications. Standard lab equipment was used to make measurements.

Table 1. Summary of main measuring instruments used and measurements made.

Measuring instrument	Make and model	Frequency range	Measurement type(s)	Notes
Spectrum analyzer	HP 8563E	9kHz-26.5GHz	Spectrum Phase noise plots* RMS phase noise Drift	*in combo with Plottergeist software
Frequency counter	Keysight 53230A	Ch.1-2 up to 350MHz Ch.3 300MHz-15GHz	Frequency Allan Deviation*	*in combo with Timelabs software
Optical spectrum analyzer	Agilent 86142B	> 50GHz	Frequency	
Power meter	HP E4418B	10MHz-18GHz	Power	

The main functions of the system are its tunable output frequency, variety of options for tuning, and ability to engage a phase-locked loop. Each function is important, as a general procedure for locking to a particular frequency is to set the desired frequency with the VCO, use the tuning functions to adjust the output signal closer to the desired frequency, then engage the PLL lockbox.

Figure 4. Measurement setups.

a) Using OEwaves internal reference.

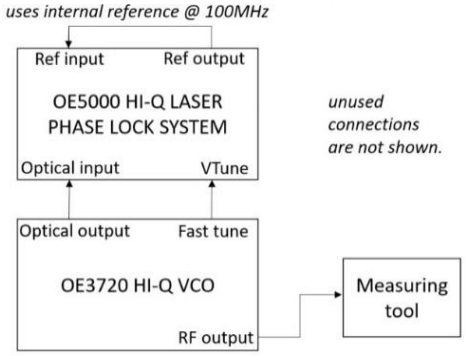

b) Using an external reference.

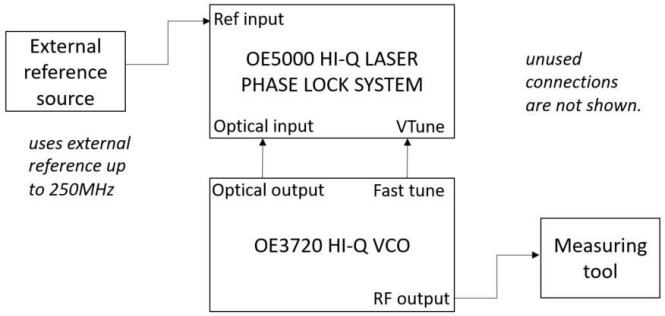

The OEwaves system can supply its own internal reference, or use an external reference. Initial verification was done with the internal reference connected. Later testing of stability and signal properties was completed with a stable external reference to see whether this resulted in improved performance.

Initial testing involved only the VCO, putting the system in "free-running" mode. A graphical user interface (GUI) was used to set a range of frequencies, and the resulting output

signal was examined using a spectrum analyzer, a frequency counter, and an optical spectrum analyzer. The multiple measurement instruments were required because the OEwaves system can produce a signal from 1-50GHz, and no single instrument could measure over that entire range. After verifying the range of output frequencies, the different methods for fine adjustments to the output signal were tested.

The output frequency can be tuned either through adjustment buttons in the GUI or by directly applying a 0-5V DC voltage to the VCO. Testing of the adjustment functionality was mostly qualitative by visually inspecting the output signal on a spectrum analyzer and observing its changes in response to applied voltage and use of the GUI adjustment buttons. With the VCO functionality verified, the PLL lockbox was then introduced.

Visual inspection on a spectrum analyzer of signal capture and the characteristics of a locked output signal verified the validity of the system's signal lock. To lock, the output signal must be within a particular capture range around the desired lock frequency. The capture range determines how much tuning needs to be done to adjust the free-running output frequency before locking. To check the capture range, the adjustment buttons were used to increase and decrease the output frequency away from the desired lock frequency until the system was no longer able to lock. After verifying that the OEwaves system was functional, testing moved on to characterization of the output signal properties, particularly those relating to noise and stability. Many of these measurements were carried out with the system both free-running and then phase-locked for comparison, with the expectation that phase-locking would show an improvement in performance.

Drift was measured by operating a spectrum analyzer in MAX HOLD mode for at least 60 seconds, then pressing VIEW HOLD. This essentially smears the signal's peak across the range of frequencies it was measured at during the duration of the MAX HOLD. From there, the MARKER DELTA function was used determine the range of frequencies spanned by the smeared peak. Drift as a rate was obtained by dividing the change in frequency by the duration of the MAX HOLD measurement.

Figure 5. Drift measurement using MARKER DELTA function of spectrum analyzer.

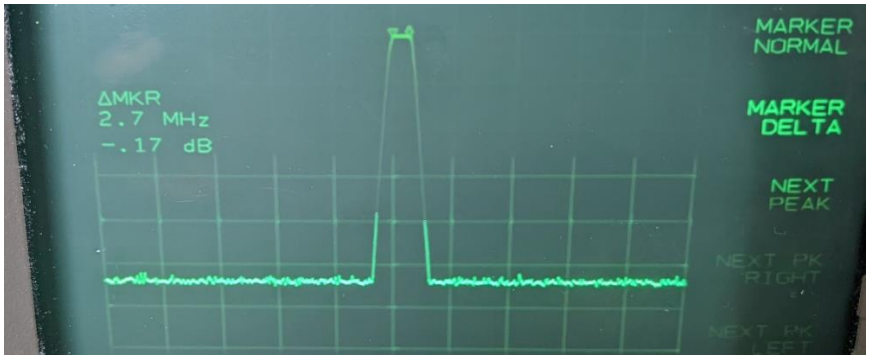

Signal spectrum after one minute of spectrum analyzer measurements. The frequency of the signal varied by approximately 2.7MHz over that time period, as determined by using the MARKER DELTA function to measure the width of the displayed spectrum's flat peak.

Phase noise and timing jitter are directly related to each other. Two methods were used to measure both characteristics. For each method, timing jitter was calculated by integration directly from a phase noise plot. Initial jitter and phase noise measurements were carried out with a phase noise utility installed on the spectrum analyzer. With the RF output connected to the spectrum analyzer input and the free-running or phase-locked signal centered on the spectrum analyzer display screen, the phase noise utility generates a log plot of phase noise against frequency offset for a specified range of offsets spanning up to five decades. This plot can be saved to a laptop by using Plottergeist software to emulate a physical printer. Within the phase utility, there is also an option to calculated integrated RMS phase noise in radians and degrees over a specified offset range. The integrated RMS phase noise in angular units was recorded by hand and converted to timing jitter in femtoseconds with a spreadsheet formula and known oscillator frequency f_O.

$$\text{RMS JITTER (seconds)} = \frac{\text{RMS PHASE JITTER (radians)}}{2\,\pi\,f_O}$$

The spectrum analyzer is not designed specifically for phase noise measurement, so phase noise plots were also generated with a phase noise test set. The test set performed an integrated phase noise jitter calculation and allowed for both plots and raw data to be saved. To determine the jitter contributed at different offset frequencies, individual evenly-spaced data points from each decade of the phase noise plot were manually estimated and entered into an online phase noise to jitter calculator. This provided the jitter for each decade of offset from the carrier frequency. Jitter from different integration ranges must be added in quadrature to correctly sum to total jitter. A spreadsheet was used to calculate the proportional contribution of each decade of offset to the total jitter.

As another measure of stability, Allan deviation was measured with the Keysight 5320A Frequency Counter in combination with Timelab software. The instrument communicated frequency readings to a laptop running Timelab over a network connection, and Timelab calculated and plotted Allan deviation. Timelab is also able to calculate and plot other measures of deviation, and export raw frequency data to a file.

Results

Testing verified that the system performs as expected with regards to its main functions. In several areas, the system outperforms its own specifications. The VCO specifications state that it can produce a tunable output frequency from 0-50GHz.

Figure 6. Free-running output frequency vs set frequency, with residuals.

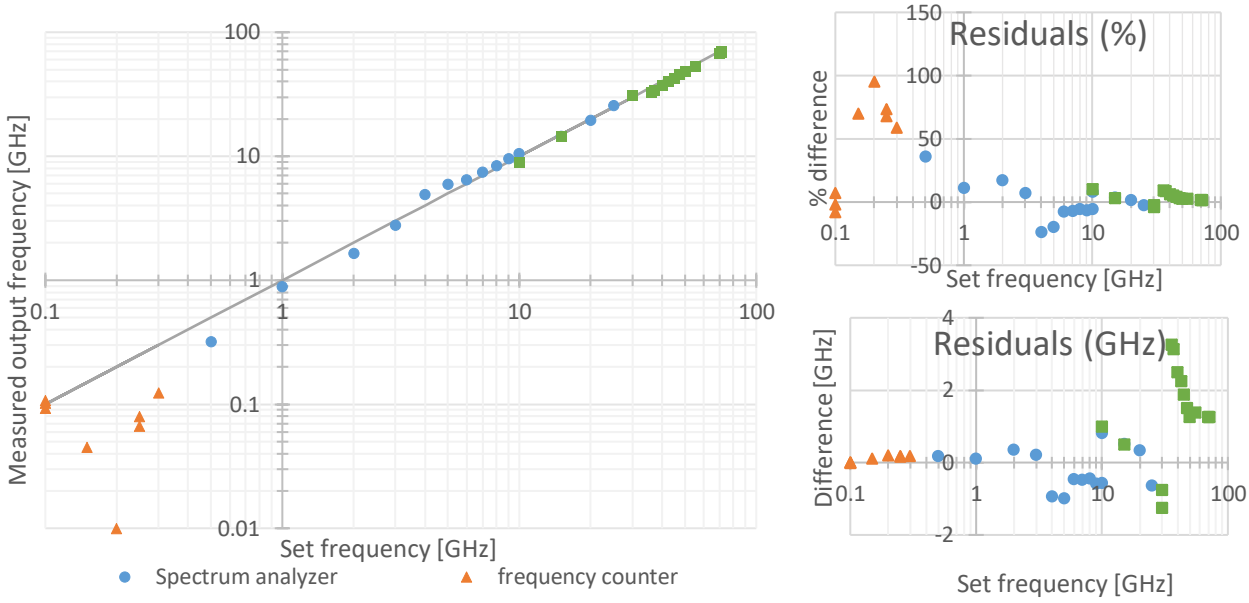

Set frequencies ranging from 0.1GHz to 72GHz are shown on the horizontal axis of all three plots. Measured free-running output frequencies in GHz are shown on the vertical axis of the left plot. The differences between measured frequencies and set frequencies, expressed in either GHz or as a percentage of the set frequency, are shown on the vertical axes of the right two plots. Log-scaled axes have been chosen to more clearly show both low and high frequencies. The instruments used to take each measurement are indicated by marker color and shape. No tuning corrections were applied to the measured frequencies.

Figure 6 shows that the measured output frequency from the free-running, uncorrected VCO fairly closely matches the set frequency. Output frequencies were measured from 0.1 to 72GHz. This extends beyond the specified output range of 0 to 50GHz. Frequencies below 0.1GHz were not formally tested, but they are not required for this application. For all measured frequencies, the differences between the measured and set frequencies are a few GHz or less. For frequencies below 30GHz, the difference is less than 1GHz. For higher frequencies, differences of a few GHz are less significant, corresponding to 10% or less of the set frequency. For lower frequencies, a difference of less than 1GHz is significant, up to 100% of the set frequency. In actual operation, these differences can be overcome by tuning.

Tunability of the output frequency through different methods was tested qualitatively. The GUI “Fast Tune” controls do adjust the measured frequency by a consistent amount—i.e., changing the set frequency in the GUI by a particular amount will consistently change the measured frequency a proportional amount. Using the provided GUI buttons changes the set frequency by 0.1GHz. Manually editing the set frequency text field in the GUI allows for finer adjustments. This “Fast Tune” method uses a piezo to change the distance between the mirrors in one of the VCO lasers, resulting in fine adjustments to the output frequency.

The analog “Slow Tune” controls perform a similar function, but are not accessible through the GUI. Instead, a 0-5V DC voltage must be applied directly through the “Slow Tune” port. Applying 0-2.5V increases the output frequency, while applying 2.5-5V decreases the

output freqency. The response is sensitive to changes on the order of millivolts or less. The best tuning results were achieved by applying 2.5V, then adjusting the applied voltage in small steps. Applying 0V or 5V immediately or changing the voltage by a large amount will cause a strong frequency correction, and the output signal can easily overshoot and get lost.

Once the measured frequency has been adjusted close to the desired lock frequency, the phase-locked loop box can be engaged through the GUI. Locking behavior was verified through visual inspection of the output signal on a spectrum analyzer. A free-running output signal visibly changes frequency on the spectrum analyzer display and is unlikely to stay at exactly the desired frequency. When the lock is engaged, the signal appears to snap to the desired frequency, and does not visibly move on the display.

Figure 7. Locked output signal at 15GHz.

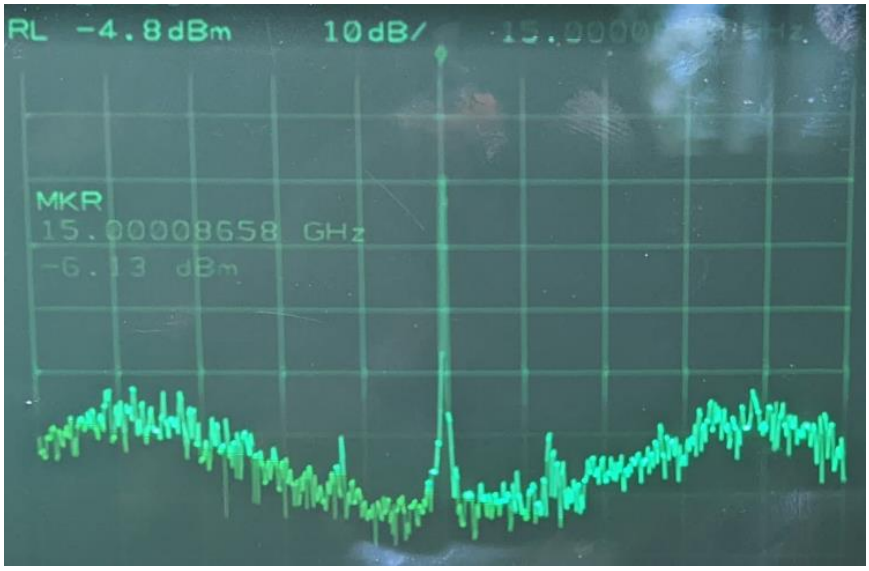

The spectrum analyzer display shows a phase-locked output signal. Frequency in GHz is shown on the horizontal axis, centered at close to 15GHz with 5kHz per division. The 20kHz loop bandwidth can be seen at 3-4 horizontal divisions. Power in dBm is shown on the vertical axis, with a reference level of -4.8dBm and 10dB per division.

Initial testing of the locking range of the system did not yield satisfactory results. Though the system did successfully lock at midrange frequencies (10GHz-17GHz), its specifications state that it should also be able to lock at frequencies down to 5GHz and up to 20GHz. This was surprising. In case the power level at low frequencies was too great and possibly saturating a detector, a 3dB attenuator was added at the optical connection between the VCO and the PLL box and locking range testing was repeated. If the issue was partially caused by saturation, including the attenuator should have extended the locking range to lower frequencies.

Figure 8. Locked output vs set frequency, before and after adding attenuator.

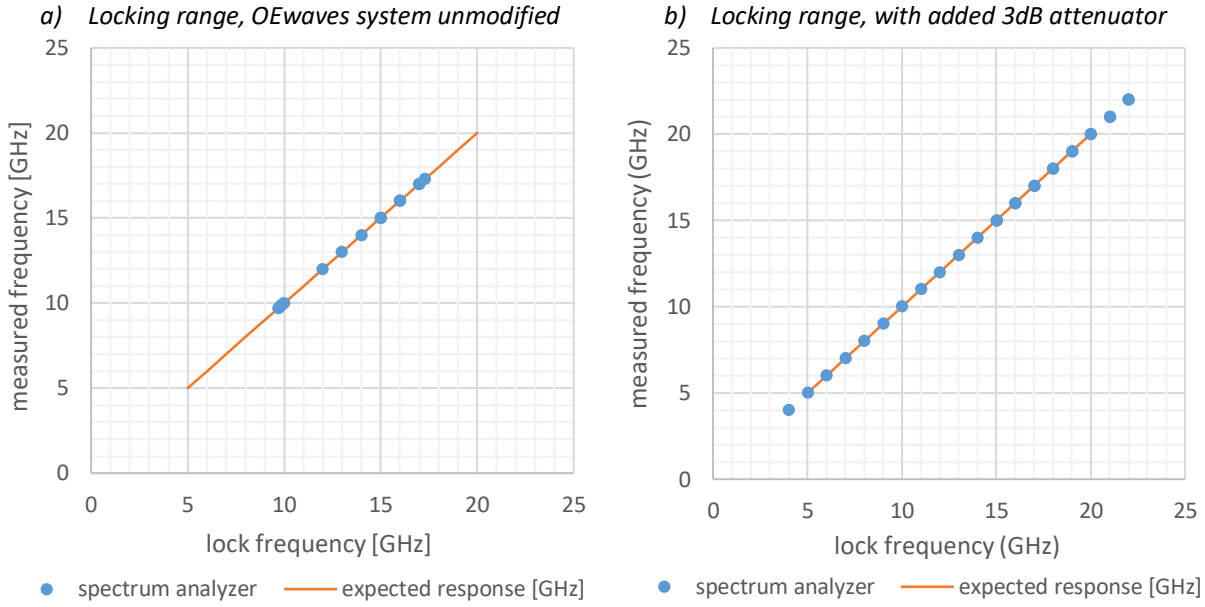

Measured phase-locked output frequencies in GHz are shown on the vertical axis. Set frequencies ranging from 4GHz to 22GHz are shown on the horizontal axis. Markers indicate measurements taken with a spectrum analyzer, while the plotted line shows the ideal lock response according to OEwaves specifications.

After adding the attenuator, the locking range of the system meets and surpasses its specifications. Specifications state that it should be able to lock from 5-20GHz. With the attenuator, it can lock from 4-22GHz. The attenuator makes a reproducible difference at both the low and high ends of the locking range. It is unclear why including an attenuator helps improve locking at higher frequencies.

It is also specified that the PLL box has a capture range of ±200MHz. A free-running output signal at a frequency within 200MHz of a carrier frequency should snap and lock to that carrier frequency with no frequency tuning required. Testing confirmed that frequencies within this range will result in successful locking, but also showed that the functional capture range is wider than specified.

Figure 9. Capture range vs set frequency

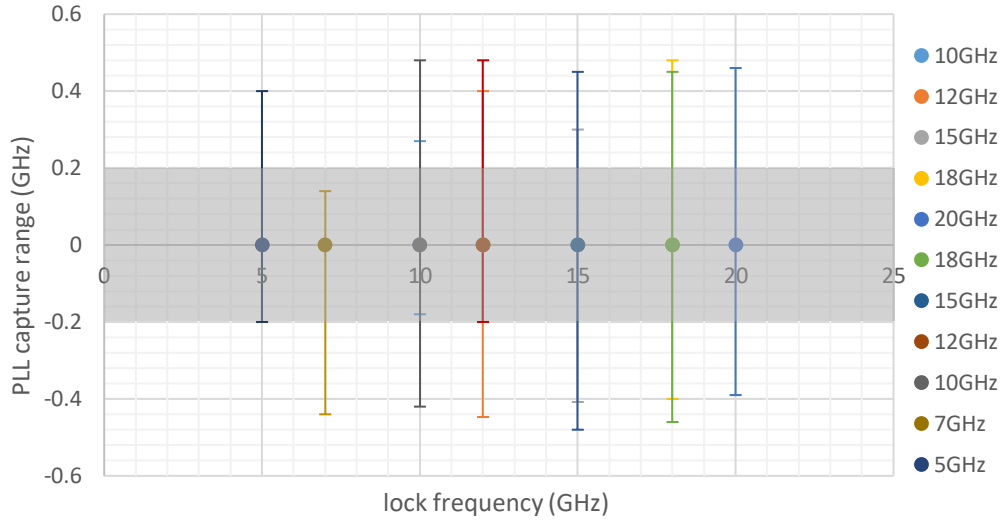

Set frequencies ranging from 5GHz to 20GHz are shown on the horizontal axis. Difference in GHz between set frequency and measured actual frequency prior to locking is shown on the vertical axis. Markers indicate a successful lock at exactly the set frequency, while vertical bars show the range of measured frequencies that still resulted in a successful lock to the set frequency. Each set of measurements is indicated with a different color. The shaded region from 0.2GHz to -0.2GHz (±200MHz around the set frequency) indicates the expected capture range.

Most of the measurement sets taken indicate a capture range of closer to ±400MHz. This means that less tuning is required prior to engaging the PLL box to lock the output frequency. Repeated measurement sets generally did not result in exactly the same capture ranges, even when taken at the same locking frequencies. This suggests that within ±400MHz of the locking frequency, capture is possible but not guaranteed. Within the capture range of ±200MHz, locking is more consistently successful.

Characterization of the locked output signal stability was more iterative than initially planned. To try and improve the stability of the system's output signal, the system was tested in several configurations: free-running (VCO only), locked using the OEwaves internal reference, locked using an external reference, and locked using an external reference with the internal reference physically disconnected from the internal circuitry. It was found that this last configuration resulted in the best performance. It is likely that the internal reference was causing interference even when not in use. In consultation with representatives from OEwaves, the PLL box was opened and a resistor was de-soldered to disconnect the internal reference.

Output signal stability was measured over several timescales. For longer timescales, frequency drift was measured at several frequencies for one minute, and then for a longer period of time. The results were averaged for ease of comparison.

Table 2. Comparison of locked and free-running signal drift.

		FREE-RUNNING		INTERNAL REF		EXTERNAL REF	
carrier frequency (GHz)	measurement duration (s)	total drift (Hz)	drift rate (Hz/s)	total drift (Hz)	drift rate (Hz/s)	total drift (Hz)	drift rate (Hz/s)
17	60	1.67e6	27833.3333	5e3	83.33333	2	0.033333
15	60	3.25e6	54166.6667	3e3	50	2	0.033333
12	60	3.42e6	57000	3e3	50	2	0.033333
10	60	2.78e6	46333.3333	2e3	33.33333	1	0.016667
12	5640 / 12900 / 6369	52e6	9219.85816	800e3	62.0155	4	0.000628
AVERAGE drift rate (Hz/s)		**38910.6383**		**55.73643**		**0.023459**	

Mode of operation impacts the frequency drift. As would be expected, the free-running VCO has the greatest amount of frequency drift. When the system is free-running, there is no correction applied to the output signal, and its frequency visibly changes over time when viewed on a spectrum analyzer. Locking the system, even to its internal reference, reduces frequency drift significantly. The output signal drifts the least when the system is locked to an external reference with the internal reference disconnected.

Figure 10. Free-running and phase-locked frequency drift.

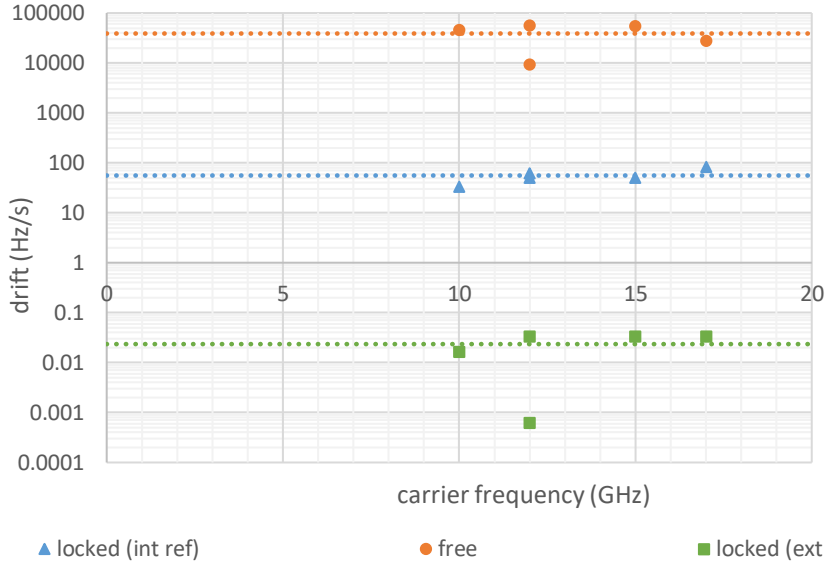

Measured drift rate in Hz/s is shown on the vertical axis. Set carrier frequencies ranging from 10GHz to 17GHz are shown on the horizontal axis. A log-scaled vertical axis been chosen to more clearly show both low and high drift rates. Marker colors and shapes indicate measurements taken in free-running or phase-locked operation. The dashed lines show the average drift for each mode of operation.

Figure 10 shows the spread of measured drift rates by carrier frequency around the calculated average drift rate for each mode of operation. Most of the measured drift rates are close to the average drift rate, with the exception of some measurements carried out over much longer timescales. Those measurements may be inaccurate (for instance, if the amount of

drift goes off the screen, then any recorded measurement would be an underestimate), or it may be that the drift rate is not constant with time.

There are consistent improvements in frequency drift as a result of locking the system, and then again as a result of disconnecting the internal reference. The free-running system outputs a signal with an average frequency drift on the order of tens of kHz per second. The locked system outputs a signal with an average frequency drift on the order of tens of Hz per second – an improvement by a factor of three orders of magnitude. With the internal reference disconnected and only an external reference used, the system outputs a signal with an average frequency drift less than one Hz per second, on the order of hundredths of Hz per second.

Phase noise is a measurement of frequency stability on much smaller timescales. Rather than a consistent drift in one direction or another, a phase noise plot will show the strength of oscillations at frequencies other than the carrier, such as different types of noise.

Figure 11. Phase noise plots, locked OEwaves output signal.

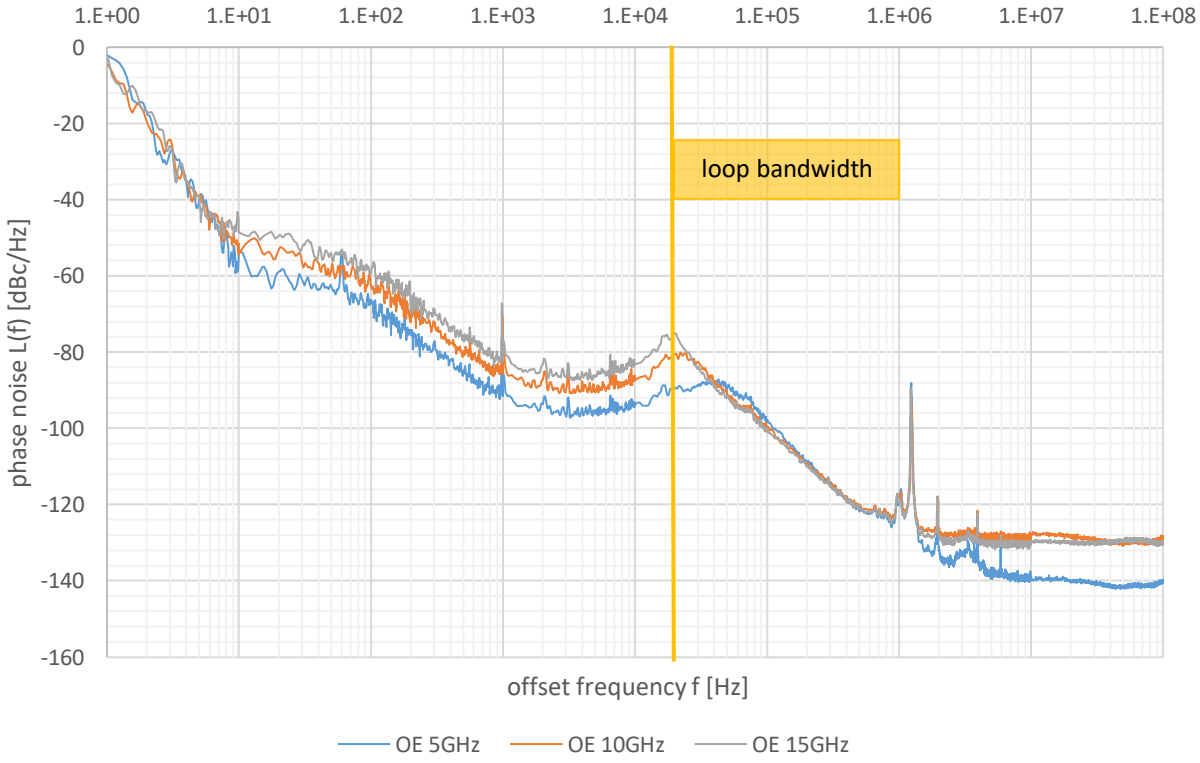

Offset from the carrier frequency in Hz is shown on the horizontal axis. Phase noise in dBc is shown on the vertical axis. The three upper traces show phase noise of a locked output signal at 5GHz (blue), 10GHz (orange), and 15GHz (gray). The 20kHz loop bandwidth is indicated with a vertical yellow line. These phase noise plots were generated after disconnecting the OEwaves internal reference and used only an external reference.

The phase noise of the output signal decreases as the frequency offset from the carrier frequency increases. This means that the strongest components of the signal are at frequencies near the desired carrier frequency. At offset ranges between 10Hz and 20kHz, there are

consistent differences in phase noise for signals at different carrier frequencies. Higher-frequency signals have higher phase noise than lower-frequency signals. 20kHz is the phase-locked loop bandwidth, so the loop works to reduce phase noise within 20kHz of the carrier frequency and has little to no effect on phase noise at frequencies further from the carrier frequency. In the phase noise plot, this is shown by the peak at 20kHz, and the similarity of the phase noise for all three carrier frequencies at frequency offsets larger than 20kHz. There are strong spurs at approximately 1kHz and 1MHz, and weaker spurs at approximately 2kHz, 3kHz, 6kHz, 2MHz, 4MHz, and 6MHz.

For a more quantitative, time-domain view of stability, phase noise plots can be converted into jitter, expressed in femtoseconds (fs). Depending on the specifications of the system, certain amounts of jitter in particular ranges of frequency offset may or may not be acceptable.

Figure 12. Proportional contributions to integrated timing jitter by offset from carrier frequency.

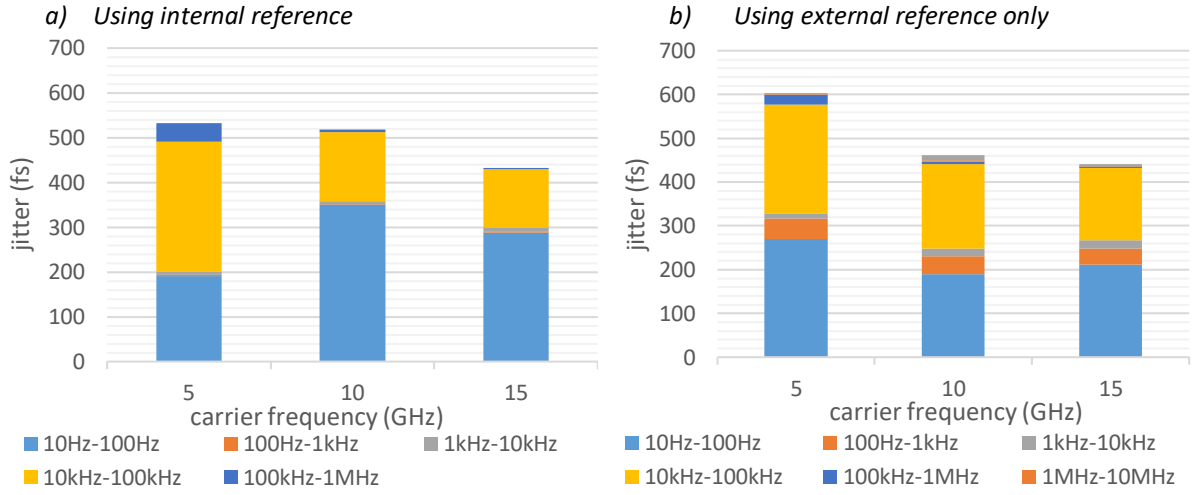

Locked carrier frequency in GHz is shown on the horizontal axis. Integrated timing jitter in femtoseconds is shown on the vertical axis. The top of each column indicates the total jitter, while the proportional contribution of each decade of offset is shown by a differently colored section of each column. The offset ranges are stacked in each column by distance from the carrier frequency—offset ranges closer to the carrier frequency at the bottom, and offset ranges farther from the carrier frequency at the top.

The leftmost plot was created using phase noise data taken with the internal reference in use. The rightmost plot was created from phase noise data taken after disconnecting the internal reference, using an external reference only. Disconnecting the internal reference did not make much of a difference to the total jitter – total jitter at 5GHz increased slightly, total jitter at 10GHz decreased slightly, and total jitter at 15GHz stayed essentially the same.

Qualitatively, the plots reveal which offset ranges contribute the most jitter. The most jitter is contributed by offset ranges 10Hz-100Hz and 10kHz-100kHz from the carrier frequency. The 10Hz-100Hz range is relatively close to the carrier frequency, so it contributes a lot of jitter. The 10kHz-100kHz range encompasses the 20kHz loop bandwidth. The loop is non-ideal, so phase noise correction is reduced at frequency offsets approaching 20kHz. Outside of the loop,

there is no phase noise correction. This reduced phase noise correction around the loop bandwidth means that the offset frequency range around the loop bandwidth will contribute more jitter. This holds true for the system both before and after disconnecting the internal reference. Allan deviation plots more clearly show the improvements in performance after disconnecting the OEwaves internal reference.

Figure 13. Allan deviation of OEwaves output before and after disconnecting internal reference

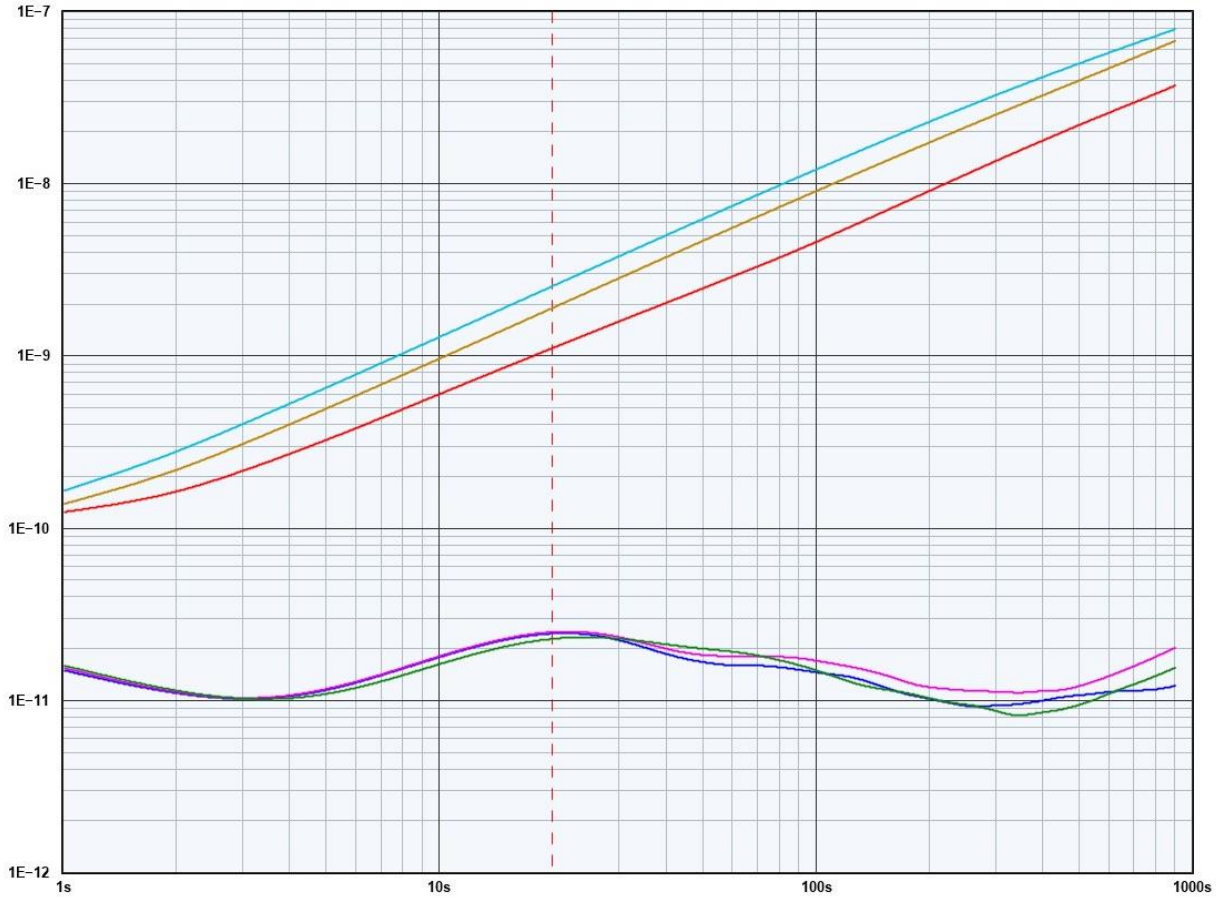

Trace	Notes	Input Freq	Sample Interval	ADEV at 20s	Duration	Elapsed	Acquired	Instrument
14GHz locked EXT REF ONLY		14000 MHz	1.000 s	2.47E-11	1h	1h	3600 pts	Agilent 53230A
10GHz locked EXT REF ONLY		10000 MHz	1.000 s	2.52E-11	1h	1h	3600 pts	Agilent 53230A
12GHz locked EXT REF ONLY		12000 MHz	1.000 s	2.30E-11	1h	1h	3600 pts	Agilent 53230A
10GHz locked		10000 MHz	1.000 s	1.13E-9	1h	1h	3600 pts	Agilent 53230A
12GHz locked		12000 MHz	1.000 s	2.59E-9	1h	1h	3600 pts	Agilent 53230A
14GHz locked		14000 MHz	1.000 s	1.94E-9	1h	1h	3600 pts	Agilent 53230A

The figure shows Allan deviation plotted for the OEwaves output signal at different frequencies. The upper three traces show Allan deviation for 12GHz (light blue), 14GHz (yellow), and 10GHz (red) using the OEwaves internal reference. The lower three traces show Allan deviation for 12GHz (green), 14GHz (dark blue), and 10GHz (magenta) using the Agilent E8257 signal generator as an external reference after disconnecting the OEwaves internal reference.

Work still needs to be done to understand and interpret the Allan deviation plots produced. However, in general, a low Allan deviation corresponds to good performance and higher stability over short timescales. The figure above clearly shows much lower and flatter

Allan deviation plots after disconnecting the OEwaves internal reference. With a good reference source, the OEwaves system's performance can be significantly improved.

Stable commercial reference

To add context to the signal stability measurements carried out on the OEwaves system, the same measurements were carried out on a very stable commercial laser synthesizer, the Agilent E8257 Analog Signal Generator. It can output frequencies from 250kHz to 40GHz, and is known to be a stable source with low phase noise.

Figure 14. OEwaves phase noise compared to Agilent E8257 phase noise

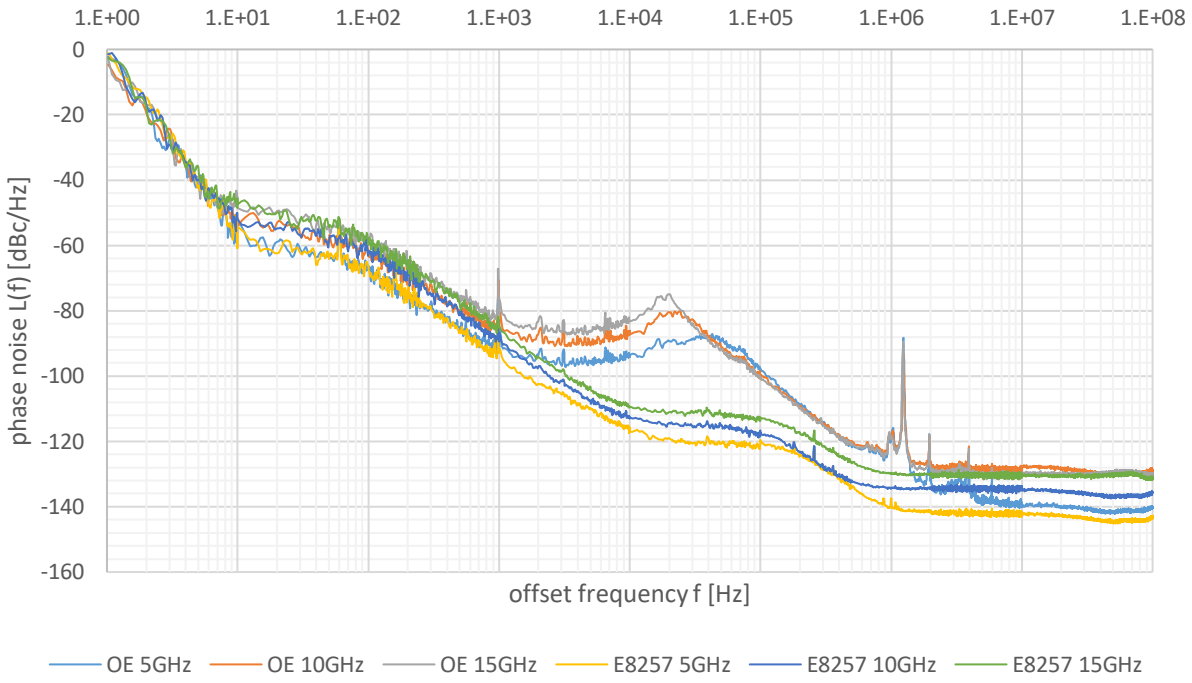

Offset from the carrier frequency in Hz is shown on the horizontal axis. Phase noise in dBc is shown on the vertical axis. The three upper traces show phase noise of a locked output signal from the OEwaves system at 5GHz (light blue), 10GHz (orange), and 15GHz (gray. The three lower traces show phase noise from the Agilent E8257 signal generator at 5GHz (yellow), 10GHz (dark blue), and 15GHz (green). These phase noise plots were generated after disconnecting the OEwaves internal reference and used only an external reference.

The phase noise plots of the two sources are comparable at small frequency offsets between 1Hz and 1kHz. Generally, the Agilent E8257 source has lower phase noise than the OEwaves system. However, close to the carrier frequency, well within the OEwaves loop bandwidth, the OEwaves system appears to perform similarly to the Agilent E8257 source. The phase noise performance of the two sources begins to vary at larger frequency offsets greater than 1kHz. The Agilent E8257 source's phase noise continues to decrease steadily from 1kHz to 10kHz, then flatten out slightly from 10kHz to 100kHz, then decrease again from 100kHz to 1MHz, then remain generally constant at offsets greater than 1MHz.

The difference in phase noise is most significant at offsets near 20kHz, the loop bandwidth. The OEwaves phase noise traces begin to flatten out at 1kHz, then increase to a peak at 20kHz. At offsets larger than 20kHz, the phase noise decreases steadily, then generally remains constant at offsets greater than 1MHz. Qualitatively, the OEwaves system performs similarly to the Agilent E8257 source except near its loop bandwidth. This is also supported more quantitatively by each source's integrated timing jitter characteristics.

Figure 15. Integrated timing jitter characteristics for OEwaves system and Agilent E8257.

a) OEwaves jitter *b) Agilent E8257 jitter*

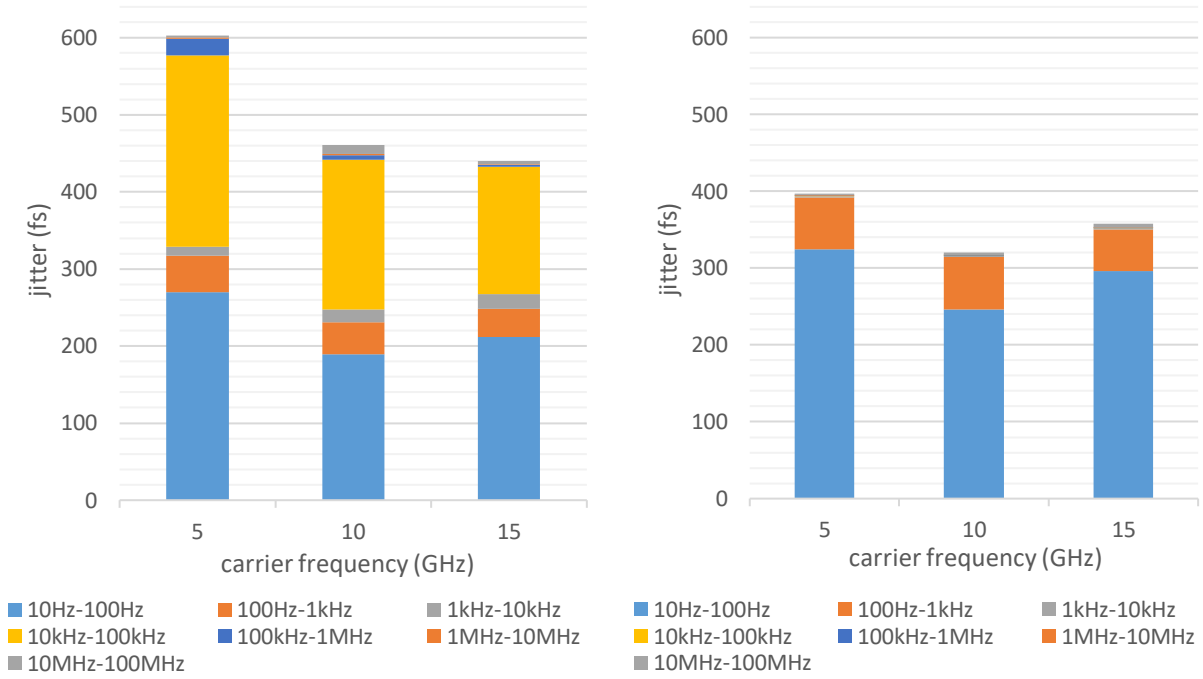

Locked carrier frequency in GHz is shown on the horizontal axis. Integrated timing jitter in femtoseconds is shown on the vertical axis. The top of each column indicates the total jitter, while the proportional contribution of each decade of offset is shown by a differently colored section of each column. The offset ranges are stacked in each column by distance from the carrier frequency—offset ranges closer to the carrier frequency at the bottom, and offset ranges farther from the carrier frequency at the top.

Both plots show the integrated timing jitter in femtoseconds for three different carrier frequencies, with differently colored column sections representing the proportional contribution of different decades of frequency offset. The leftmost plot shows the timing jitter for the OEwaves source, while the rightmost plot shows the timing jitter for the Agilent E8257 source. Total jitter is consistently higher for the OEwaves source than for the Agilent E8257 source. However, this is largely due to contributions from the 10kHz-100kHz decade of frequency offsets. The 20kHz loop bandwidth is responsible for the added jitter. If contributions from 10kHz-100kHz offsets were removed or reduced, the OEwaves source would have significantly improved jitter, approaching that of the Agilent E8257 source.

A difference in performance between the OEwaves source and the Agilent E8257 source can also be noted in the output power characteristics over long timescales.

Figure 16. Output power over time.

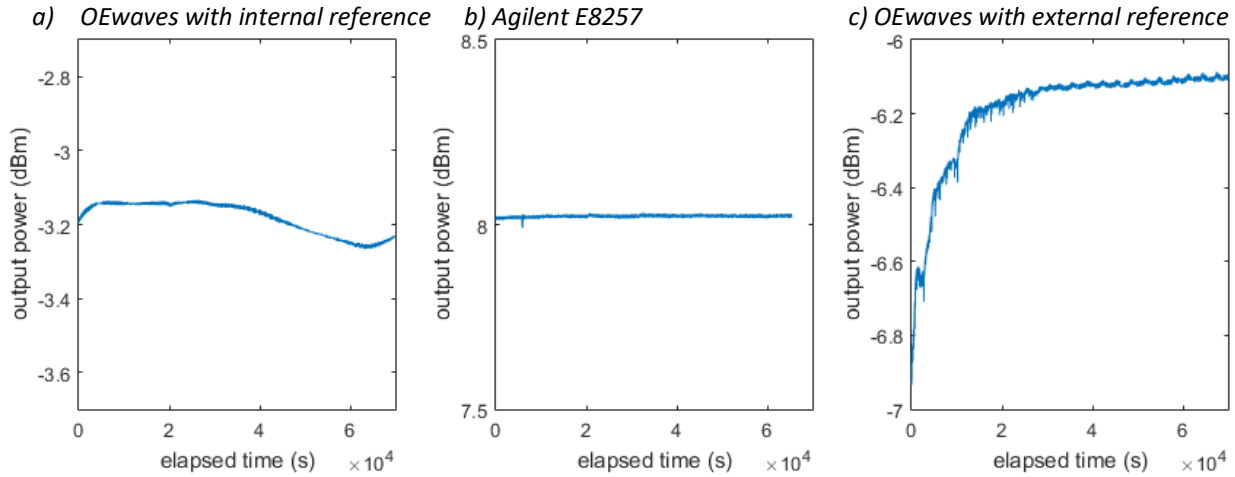

The leftmost figure shows the output power over a 19hour time period of the locked OEwaves system using its internal reference. The middle figure shows the output power over a 19hour time period of the Agilent E8257 signal generator, used as a laser synthesizer reference for ALMA. The rightmost figure shows the output power over a 19hour time period of the locked OEwaves system using the Agilent E8257 as an external reference, with the internal reference disconnected. The vertical axes are output power in dBm. The horizontal axes are time in seconds. All three figures span 1dBm along the vertical axis, and 7x10^4 seconds (approximately 19hours) along the horizontal axis.

The power output of the Agilent E8257 appears more stable over time than that of the OEwaves system. Each source/configuration remained within 1dBm over 19hours, but the Agilent E8257 had much less variation than the OEwaves system. Further characterization would be required to draw more conclusions, as there were external factors such extreme weather and possible interference from ventilation. These factors were not controlled when taking data for this project, but could have impacted the results displayed in Figure 10.

Performance compared to application requirements

The OEwaves system is primarily under consideration for use with the ngVLA project. However, it could be considered for future radio telescope projects as well. To put it in context, the OEwaves system was compared to current ngVLA requirements as well as the local oscillator used for ALMA, the full local oscillator chain for ALMA, and the commercially available Agilent E8257 Analog Signal Generator.

Table 3. Comparison of ngVLA requirements to ALMA, Agilent E8257, and OEwaves.

	ngVLA LO requirement	ALMA Laser Synthesizer	ALMA Full LO	Agilent E8257	OEwaves
Frequency Range (GHz)	5.8-113.1	27-122	27-938	0-20	1-50 Measured 1-70
Output Power	13 dBm (20 mW)	6 dBm (4 mW) optical	17 dBm (50 mW)	20 dBm (100 mW)	-7 to -2 dBm (0.2-0.6 mW)
Phase Noise		122 GHz dBc/Hz	122 GHz dBc/Hz	10 GHz dBc/Hz	15 GHz dBc/Hz
100 Hz	TBD	-62	-62	-95	-60
1 kHz	TBD	-73	-73	-114	-80
10 kHz	TBD	-93	-93	-114	-82
100 kHz	TBD	-95	-95	-118	-100
1 MHz	TBD	-100	-98	-145	-122
10 MHz	TBD	-80	-128	-160	-130
Integrated Noise (jitter)					
10 Hz - 10 MHz	76 fsec	< 57 fsec	<63 fsec	< 38 fsec	438 fsec
1 kHz - 10 MHz	N/A	< 27 fsec	<38 fsec	< 30 fsec	287 fsec

The OEwaves system does not fully meet any of the quantitative requirements for an ngVLA local oscillator. It does not generate high enough frequencies. It does not output enough power, though this could be addressed with additional components. No numerical phase noise requirements for an ngVLA LO have been finalized. The OEwaves phase noise measurements are comparable to the phase noise of ALMA's local oscillator and laser synthesizer at offsets not near the 20kHz loop bandwidth. The OEwaves system does not meet the ngVLA jitter requirement and does not compare favorably to the other sources in the table.

Conclusions

Findings in the lab indicate that the OEwaves system performs well for a microwave photonic source. Its performance meets or exceeds many of the specifications provided by OEwaves. It can output frequencies from 0-50GHz, successfully lock to any set frequency from 5-20GHz, and quickly lock within 200MHz of the desired frequency. In its optimal configuration, it exhibits very low long-term frequency drift. Within its 20kHz loop bandwidth, phase noise and timing jitter are well controlled.

There are still several areas in which the OEwaves system may fall short of requirements for use in future radio antenna local oscillators. Current specifications for ngVLA (and comparable specifications for ALMA) require a local oscillator to be able to lock at frequencies greater than 100GHz. The OEwaves system tested in this project can only lock at frequencies up to 20GHz, though it can output free-running signals at frequencies up to 70GHz. It is possible a unit with higher locking frequencies could be developed and purchased, but this would significantly increase the cost of the unit. Though the exact phase noise requirements for ngVLA

are not yet determined, the measured phase noise for the OEwaves system performs poorly around its 20kHz loop bandwidth when compared to well-characterized, stable systems. This poor phase noise performance results in a great deal of timing jitter, which does not meet the ngVLA jitter requirement of 76fsec from 10Hz to 10MHz. The OEwaves system has over 400fsec of jitter from 10Hz to 10MHz.

It is worth noting that the OEwaves system is still in an early stage of development. OEwaves has indicated a desire to meet requirements for use with ngVLA and a willingness to develop the system further to better meet requirements. The current problems with the OEwaves systems could be addressed with more refinement of components and design.

There are some sources of uncertainty in this analysis. Mainly, the testing procedures carried out are not particularly rigorous. Tests were performed in an uncontrolled environment on a lab bench, so factors such as variations in ambient temperature, pressure, and humidity could have impacted performance of the OEwaves system and the measurement instruments from day to day. The amount of time that the equipment was on and the order of the tests performed were not controlled, so different levels of equipment use and warmup/cooldown time also could have impacted performance. The instruments used to make measurements were past due for recalibration, so the sensitivity and accuracy of the data gathered may have been lower than expected. The OEwaves system itself also contributed some uncertainty. Its performance indicators, such as an LED indicating the success of a phase lock, were not always accurate. There were occasional irreproducible bugs, and some issues that, while resolved, were not definitively traced to a cause.

It is possible that the phase noise and jitter of the OEwaves system can be improved by increasing its loop bandwidth. This can be done by adjusting the electrical components that control the loop bandwidth. Additional modifications were made in the lab to improve performance, such as adding a 3dB attenuator and disconnecting the OEwaves internal reference. Work could be done alongside OEwaves to incorporate those modifications into future commercially available designs of the system.

Further testing of the OEwaves source could also be done to gain a better understanding of its stability, power output, performance under stress, and performance in a more complex system better approximating a real-life use case. Further testing in a more rigorous and controlled environment would be beneficial. The OEwaves source could also be tested with an existing telescope, such as the Green Bank Telescope, by swapping out an existing local oscillator and evaluating whether observations can still be made with the OEwaves source used as the local oscillator.

The OEwaves system is currently considered as a backup method for ngVLA. The work done this summer does not indicate good enough performance for use as a primary method in its current configuration. With additional development to address stability concerns, and

additional testing, the OEwaves RF photonic source could be a viable local oscillator option in future radio telescope antenna designs.

Acknowledgements

Many thanks to Bill Shillue, Christophe Jacques, Jason Castro, and Jim Muehlberg for their invaluable support and guidance with this project. I would also like to acknowledge Lute Maleki and Robert Moss for their technical support and debugging assistance on behalf of OEwaves. Finally, my research this summer at the National Radio Astronomy Observatory (NRAO) was made possible through the NRAO REU program. (Research Experiences for Undergraduates). Thank you to Jim Braatz and all others involved in running summer student programs at NRAO.

References

Brundage, W. *Back End Procedure for Calculating Allan Standard Deviation ASDy(2,T,τ)*. Version A, BEND-50.00.00.00-324-A-PRO, National Radio Astronomy Observatory, 27 Oct. 2010.

Collins, Ian. *Phase-Locked Loop (PLL) Fundamentals*. Analog Dialogue, July 2018.

Condon, James J., and Scott M. Ransom. "Chapter 3: Radio Telescopes and Radiometers." *Essential Radio Astronomy*, National Radio Astronomy Observatory, 15 Oct. 2015.

Jitter and Phase Noise. Seiko Epson Corporation.

Kester, Walt. *Converting Oscillator Phase Noise to Time Jitter*. Analog Devices, Oct. 2008.

Long, S. *Phase Locked Loop Circuits*. UCSB/ECE Department, 27 Apr. 2005.

Mastering Phase Noise Measurements. Rohde & Schwarz, Oct. 2016.

Phase Noise Measurement Solutions Selection Guide. Keysight Technologies, 26 Jan. 2018.

Phase Station 53100A User's Manual. Revision 1.04, Phase Station, 25 Apr. 2022.

Photonic RF Source: Voltage Controlled Oscillator (VCO) Laser Lock Box Operating Manual. Revision A, MAN-0007, OEwaves, 2021.

PLL Phase Locked Loop Tutorial & Primer. electronics-notes.

Plottergeist - HPGL Plotter and PCL Printer Emulator software. Aphena.

PROPOSAL SOW: NRAO to OEwaves. National Radio Astronomy Observatory, 3 Nov. 2021.

Ramian, F. *Time Domain Oscillator Stability Measurement Allan variance*. Rohde & Schwarz, Apr. 2015.

Saini, K. *Notes on the measurement of amplitude stability ("Allan Variance" of output power) of the ALMA First LO driver assemblies.* ALMA EDM, FEND-40.10.00.00-041-A-VER, National Radio Astronomy Observatory, 16 Sept. 2004.

Shillue, B., and Y. Masui. *Laser Synthesizer Phase Noise Measurement Test Data Report*. Version A, BEND-56.11.00.00-020-A-TDR, National Radio Astronomy Observatory, 7 June 2010.

"Tutorial: All about Frequency Synthesis." *Maxim Integrated*, 20 Mar. 2019.

Vernotte, François. *Variance Measurements: Practical Use - Statistics - Long Term Prediction*. 2011 Joint Conference of the IEEE International Frequency Control Symposium & European Frequency and Time Forum, May 2011.